Investigating Crack Initiation and Propagation of Concrete in Restrained Shrinkage Circular/Elliptical Ring Test

Wei Dong · Xiangming Zhou · Zhimin Wu · Bohan Xu

W. Dong · Z.M. Wu · B.H. Xu

State Key Laboratory of Coastal and Offshore Engineering, Dalian University of Technology, Dalian 116024, P. R. China.

W. Dong (Corresponding author)

Tel: +86-411-84707414.

E-mail: dongwei@dlut.edu.cn.

X.M. Zhou

Department of Mechanical, Aerospace and Civil Engineering, Brunel University London, Uxbridge, Middlesex UB8 3PH, United Kingdom & State Key Laboratory of Coastal and Offshore Engineering, Dalian University of Technology, Dalian 116024, P. R. China.

Abstract

The restrained ring test, which is recommended by AASHTO and ASTM, has been used for assessing the potential of early-age cracking of concrete and other cement-based materials. Recently, a novel elliptical ring test method has been proposed to replace the circular ring test method for the purpose of shortening ring test duration and observing crack initiation and propagation more conveniently. In order to explore the mechanism of this novel test method, a numerical model is developed to analyze crack initiation and propagation process in restrained concrete rings, in which the effect of concrete shrinkage is simulated by a fictitious temperature drop applied on concrete causing the same strain as that induced by shrinkage. First, an elastic analysis is conducted to obtain the circumferential stress contour of a concrete ring subject to restrained shrinkage. Combined with the fictitious crack model, a fracture mechanics method is introduced to determine crack initiation and propagation, in which crack resistance caused by cohesive force acting on fracture process zone is considered. Finite element analysis is carried out to simulate the evolution of stress intensity factor (SIF) in restrained concrete rings subject to circumferential drying. Cracking age and position of a series of circular/elliptical concrete rings are obtained from numerical analyses which agree reasonably well with experimental results. It is found that the sudden drop of steel strain observed in the restrained ring test represents the onset of unstable crack propagation rather than crack initiation. The results given by the AASHTO/ASTM restrained ring test actually reflects the response of a concrete ring as a structure to external stimulation, in this case restrained concrete shrinkage.

Keywords *concrete; early-age cracking; restrained shrinkage; fracture mechanics; crack propagation process; elliptical ring test.*

40 **Abbreviations**

a : crack length

A : exposed surface area of a concrete element

d : steel ring thickness

E : elastic modulus of concrete

f_c : uniaxial compressive strength

f_t : splitting tensile strength of concrete

G_F : fracture energy

K_I^S : stress intensity factor caused by applied load

K_I^σ : stress intensity factor caused by cohesive force

R_0 : inner diameter of circular concrete ring

R_1 : major semi-axes of inner circumference of elliptical concrete ring

R_2 : minor semi-axes of inner circumference of elliptical concrete ring

t : age of concrete

V : volume of a concrete element

w : crack opening displacement

w_0 : stress-free crack opening displacement

w_s : displacement corresponding to the break point in bilinear σ-w relationship

Δa : crack growth length

ΔP : load incensement

σ : cohesive stress

σ_s : stress corresponding to the break point in bilinear σ-w relationship

41

Introduction

Autogenous, drying or thermal shrinkage often occur in concrete elements or structures, resulting in volume changes of concrete. If volume changes of concrete are restrained, tensile stress may be developed in concrete [1, 2]. Since concrete's low tensile strength provides little resistance to tensile stress, cracking may occur when the developed tensile stress in concrete excesses its tensile strength. These restrained shrinkage cracks are often observed in concrete elements and structures with high surface area-to-volume ratio such as industrial floors, concrete pavements and bridge decks [3]. Cracking in concrete may reduce load carrying capacity, shorten the service life of concrete structures, and accelerate deterioration resulting in increased maintenance costs. Therefore, it is significant to assess cracking potential of concrete mixtures under restrained shrinkage in service.

The restrained circular ring test has been widely used for assessing cracking tendency of concrete and other cement-based materials due to its simplicity and versatility [1, 4-10]. As a standard test method for assessing cracking potential of concrete mixtures under restrained condition, the circular ring test has been recommended by AASHTO (i.e. AASHTO T334-08: *Standard Method of Test for Estimating the Cracking Tendency of Concrete*) and ASTM (i.e. ASTM C1581/C1581M-09a: *Standard Test Method for Determining Age at Cracking and Induced Tensile Stress Characteristics of Mortar and Concrete under Restrained Shrinkage*). Accordingly, in restrained ring test, the effects of specimen size/geometry [11-13]; and moisture gradients and drying condition [12-14] on cracking of concrete or other cement-based materials have been studied. Moreover, novel elliptical ring geometries have been adopted to replace circular ring geometries for investigating

shrinkage cracking of mortar and concrete under restrained condition[15-19]. It is generally regarded that, due to stress concentration caused by geometry effect, cracks initiate earlier in elliptical ring specimens than in circular ones though this has yet been validated in those studies. In contrast with the fact that a crack may initiate anywhere in a circular ring specimen, it tends to initiate at certain position in an elliptical ring specimen for a given ring geometry. Therefore, elliptical ring specimens have been employed for assessing cracking tendency of cement-based materials as an improved ring test by some researchers [15-19].

On the other hand, in order to study the mechanism of concrete cracking in restrained circular ring specimens, many theoretical methods have been proposed to predict cracking age of concrete. These methods can be classified as stress analysis approach [12-14, 20-22] and fracture resistance curve approach [9, 11, 23, 24]. In conventional stress analysis approach, cracking age could be obtained by comparing the residual stress in a concrete ring and its tensile strength. However, some researchers [9, 11, 23, 24] pointed out that tensile strength-based failure criterion might not yield accurate results for cracking of concrete at early ages, and a fracture-based failure criterion could appear more appropriate. In this case, the fracture resistance curve approach, which is based on fracture mechanics concepts with consideration of the energy balance, has been widely used by many researches [9, 11, 23-28]. By comparing the energy release rate (R-curve) with crack driving energy (G-curve), the onset of crack propagating unsteadily in a restrained concrete ring can be determined. It should be noted that the two methods mentioned above have also been used for predicting cracking ages of concrete in restrained elliptical ring tests [29, 30].

Although the fracture resistance curve approach provides a better explanation for what observed in restrained circular/elliptical ring test, it was generally used to predict the

92 critical cracking condition in rings subject to restrained shrinkage. Meanwhile, in
93 restrained circular/elliptical ring test, the age of cracking can be detected from the
94 sudden drop to almost zero in the measured strain of the inner restraining steel ring.
95 Further, the relationship of steel strain and actual residual stress in circular ring test was
96 derived to assess the risk for cracking [31] and to determine the crack growth status in
97 fiber concrete [32]. Generally speaking, concrete is regarded as quasi-brittle material,
98 and there are three distinguished stages in crack propagation process of concrete, i.e.
99 crack initiation, stable propagation and unstable propagation. Restraint disappearing
100 from a steel ring does not suggest the whole crack growth process, i.e. crack initiates
101 and propagates throughout a concrete ring wall.

102 In line with this, the objective of this paper is to investigate crack initiation and
103 propagation process of concrete under a restrained shrinkage condition, demonstrating
104 the failure mechanism and presenting the quantitative assessment of cracking resistance
105 for concrete in the ring test. By introducing the fictitious crack model [33], the nonlinear
106 properties of concrete, characterized by the cohesive force acting on the fictitious crack,
107 is considered. The existence of the cohesive effect reflects the strain localization and
108 nonlinear properties of quasi-brittle materials like concrete, which is an essential
109 difference between quasi-brittle and brittle materials. Meanwhile, by establishing the
110 equilibrium relationship between the crack driving effect caused by the drying
111 shrinkage and the cracking resistance caused by the quasi-brittle properties of concrete,
112 the crack development and evolution processes are elabrated. Further, the difference
113 between the cracking resistance of concrete, which is represented by the crack initiation,
114 and the structural response under a time-dependent drying stimulation, represented by
115 the unstalbe crack propagation, is clarified. It is expected that the nonlinear fracture
116 mechanics-based numerical model developed in this study will be helpful in exploring

the mechanism of restrained circular/elliptical concrete ring test which can be employed for assessing the cracking tendency of concrete and other cement-based materials.

Firstly, a numerical approach was developed in this paper to simulate the shrinkage behavior of concrete in restrained ring specimens subject to drying from their outer circumferential cylindrical surface. A fictitious temperature field, which is derived based on free shrinkage data of concrete prisms, was applied on concrete ring specimens in numerical analyses to simulate the mechanical effect of concrete shrinkage on rings under restrained condition. A crack propagation criterion based on the nonlinear fracture mechanics is introduced to determine the crack propagation, in which crack begins to propagate when the stress intensity factors (SIF) K_{I}^{S} caused by the applied load (i.e., shrinkage effect in case of concrete rings under restrained condition) exceeds K_{I}^{σ} caused by the cohesive stress. Using the proposed method, the whole fracture process including crack initiation, stable and unstable propagation is simulated, and the SIF variations at the different crack propagation stages are analyzed.

2 Experimental Program

The mix proportion for the concrete used for this study was 1:1.5:1.5:0.5 (cement: sand: coarse aggregate: water) by weight, and the maximum of aggregate size was 10 mm.

2.1 Materials Properties

Mechanical properties of concrete, such as elastic modulus E, splitting tensile strength f_{t} and uniaxial compressive strength f_{c}, at different ages were measured using 100 mm diameter and 200 mm height cylindrical specimens in this study. After curing

in sealed cylindrical moulds in normal laboratory environment for 24 h, the cylindrical specimens were de-moulded and moved into an environment chamber with 23℃ and 50% relative humidity (RH) for curing till the desirable ages of testing.

Regression analyses were conducted on the experimental data to obtain continuous functions that can represent the age-dependent mechanical properties, in this case, E and f_t, for the concrete. It was found that elastic modulus, E, of the concrete at early ages can be predicted using Equation 1.

$$E(t)=0.0002t^3-0.0134t^2+0.3693t+12.715 \quad (t\leq 28) \quad (1)$$

Splitting tensile strength, f_t, can be predicted using Equation 2.

$$f_t(t)=1.82t^{0.13} \quad (t\leq 28) \quad (2)$$

In both equations, t is the age (unit: day) of concrete. The values of E and f_t for concrete at other ages which were not directly measured can be obtained from Eqs. (1) and (2).

2.2 Free Shrinkage Tests

Free shrinkage was measured on concrete prisms with the dimensions of 280 mm in length and 75 mm square in cross section, conforming to ISO 1920-8, subject to drying in the same environment as for curing concrete cylinders. Their longitudinal length change was monitored by a dial gauge, which was then converted into shrinkage. Considering that concrete shrinkage depends on the exposed surface area-to volume (A/V) ratio, four different exposure conditions, i.e. four different values of A/V, were

166 investigated in this study. They are all surfaces sealed, all surface exposed, two side
167 surfaces sealed and three side surfaces sealed, respectively. It should be noted that side
168 surface refers to the surface with the dimensions of 280×75 mm^2. In experiment,
169 double-layer aluminum tape was used to seal the desired surfaces which were not
170 intended for drying. A two side surfaces sealed prism in free shrinkage test is shown in
171 Figure 1. Initial measurement was carried out immediately after the concrete prisms
172 were de-molded at the age of 1 day and the measurements were continuously recorded
173 twice per day until 28 days. Figure 2 shows the measured free shrinkage strain of
174 concrete at various ages under different exposure conditions.
175 It should be noted that the computation of free shrinkage strain in a concrete ring is an
176 approximate estimation for the purpose of simplification, which match the geometry of
177 the prism to the ring through the ratio of A/V. A more complex and accuracy approach
178 was introduced in Reference [28]. The free shrinkage prisms had an identical volume
179 to surface ratio to that of a short concrete ring with the depth of 75 mm when drying
180 from the top and bottom surfaces. Therefore a direct correlation can be made with the
181 shrinkage properties of the ring. In the case of tall rings drying from outer surface, the
182 shrinkage strain of concrete can be derived by introducing the average humidity profiles
183 and the relationship between shrinkage and relative humidity.
184

185 ***2.3 Restrained ring test***

186 In order to investigate the effects of the inner steel core on cracking age of
187 restrained concrete rings and the mechanism of restrained ring test, two kinds of steel
188 core, which are circular and elliptical, were investigated in current experiment program.

A circular concrete ring with its inner diameter is denoted as R_0 (see Figure 3a), and an elliptical concrete ring, with the major and minor semi-axes of its inner circumference is denoted as R_1 and R_2, respectively (see Figure 3b). According to the study of Zhou et al. [30], compared with traditional circular concrete rings, elliptical concrete rings with R_1/R_2 between 2 and 3 can provide higher degree of restraint leading to shorter cracking period in restrained shrinkage ring test so that to accelerate ring test. Therefore, in this study, for the concrete elliptical ring specimens with a 37.5 mm-thick wall same as that recommended by ASTM C1581/C1581M-09a, the inner major radius, R_1, was chosen as 150 mm and the inner minor radius, R_2, as 75 mm while the radius, R_0, of the inner circumference of the circular rings was designed as 150 mm same as R_1. The wall thickness of restraining steel cores and the height of the specimens were as 12.5 and 75 mm, respectively. Following ASTM C1581/C1581M-09a protocol, the top and bottom surfaces of ring specimens were sealed using two layers of aluminum tape and drying was only allowed through the outer circumferential cylindrical surface of the concrete rings. The test setup and sealed specimens are shown in Figure 4. The strain gauges were then connected to the data acquisition system, and the instrumented ring specimens were finally moved into an environmental chamber after the first day curing for continuous drying under the temperature 23°C and RH 50% till the first crack occurred.

It should be noted that, according to Radlinska et al. [34], specifying the precision of the restrained ring test in terms of standard deviation of measured strain is more promising than of the age of cracking. It is because the variability in the cracking age shows time dependence and it is much higher for the cracking occurred at later age. However, in this study, the cracking age was used to reflect the time-dependent material properties rather than the variability of the ring test. Therefore, it is still employed in

this study to compare the cracking tendency of concrete in elliptical and circular ring tests.

3 Numerical Modeling

3.1 Modeling of Restrained Shrinkage

In current research, a derived fictitious temperature field is applied to concrete to represent the mechanical shrinkage effect so that a combined thermal and structural analysis can be adopted to analyze cracking in a concrete ring specimen caused by restrained shrinkage. The restrained circular ring test is recommended by AASHTO and ASTM, for assessing the cracking tendency of concrete under a restrained drying shrinkage condition. However, in the case of concrete deformation caused by large temperature variation, the conventional ring test cannot serve the purpose because the restraining effect varies with the steel ring dimensions caused by varying temperature. Particularly, the restraint will disappear if the concrete expansion occurs under elevated temperature. To overcome these limitations, the dual ring test was proposed by Schlitter et al. [35-37], in which invar with a very low thermal expansion coefficient was used to make the central restraining steel ring. Meanwhile, the autogenous shrinkage can be reduced or eliminated by controlling the temperature reduction in a concrete ring, so that the remaining stress capacity of concrete can be better assessed. The research conducted by Schlitter et al. [35-37] extends the application of the restrained ring test and provide an improved understanding of the cracking potential of a cement mixture. However, it should be noted that the fictitious temperature drop proposed in this study is to numerically simulate the concrete shrinkage effect under drying, as opposed to a real temperature drop experienced in a ring test. For the purpose of the analyses, there

239 is no fictitious temperature drop enforced on the central restraining steel ring therefore
240 it makes no difference whether traditional steel or invar steel is used for making the
241 central restraining steel ring.

242 With the implementation of the fictitious temperature field, shrinkage of concrete
243 caused by the temperature field is restrained by the inner steel core, resulting in
244 compressive stress developed in the steel core and tensile stress in the concrete ring.
245 The derivation of the fictitious temperature field is elaborated elsewhere [30]. As the
246 result of this exercise, Figure 5 presents the derived relationship between fictitious
247 temperature drop and A/V ratio at 2 days interval for a concrete element irrespective of
248 its geometry/shape. It should be noted that although Fig. 5 only presents the curves at
249 2 days interval, fictitious temperature drop was actually calculated for each day which
250 was then used to update the input data for FE analyses of concrete rings in this study.
251 For a given concrete ring with certain exposure condition (i.e. certain A/V ratio), the
252 relationship between fictitious temperature drop and concrete age can be derived by
253 linear interpolation from the relationship between A/V ratio and concrete age obtained
254 in Figure 5.

255

256 ***3.2 Crack initiation and propagation***

257 According to experimental observation, in case of a thick ring (i.e., the ring wall
258 thickness is 75 mm), cracking initiates at the outer circumferential surface of a
259 restrained concrete ring, which accords well with the findings of Hossain and Weiss
260 [13] by acoustic emission testing. In case of a thin ring, to the best of the authors'
261 knowledge, there is no explicit experimental evidence that can support whether a crack
262 initiates at its outer or inner circumferential surface. Moon and Weiss [12] studied the
263 residual stress distribution in both thick and thin circular rings by considering the

moisture gradient across a concrete ring wall. Based on their results, tensile stress is the highest on the outer circumference of a concrete ring. Due to this, cracking always initiates at the outer circumference surface of a concrete ring when drying from its outer circumferential surface, no matter how thick a concrete wall is if the moisture gradient is taken into account in analyses. It is because that the moisture gradient is very significant with the majority of the drying taking place from the outer circumference of a concrete ring at early ages (i.e. low value of γ, where γ is the product of the moisture diffusion coefficient and drying time). Under this condition, the crack in a restrained concrete ring will be mainly caused by the self-shrinkage due to the moisture gradient rather than from restraining effect from the central steel ring. However, it makes sense that the crack initiation is resulted from the restraining-dominated effect from the central steel ring in case of a thin-wall concrete ring. In which case, the crack will initiate at the inner circumference of a concrete ring. Meanwhile, by considering that a thin ring has a larger A/V ratio than a thick one when drying from its outer circumference surface, the moisture gradient across a thin ring wall can be ignored and the approximate uniform shrinkage across it is assumed. However, it should be noted that it is necessary to further examine the initial crack position of a thin ring under outer circumferential surface drying from experiment.

In this study, cracks are assumed to initiate when the maximum circumferential tensile stress of concrete exceeds its tensile strength f_t. According to the experimental and numerical results conducted by Zhou et al. [30], crack randomly initiates at the inner circumference of a circular ring specimen. While in the case of an elliptical ring specimens with R_1=150 mm, R_2=75 mm, crack initiates close to the vertices on the major axis of the inner elliptical circumference (See Figure 6). Therefore, after crack initiation, a pre-crack, with the length of 2 mm, is set at the position where the

maximum circumferential tensile stress occurs. In order to consider the softening behavior in micro-cracks, the fictitious crack model [33] is introduced in the fracture analysis through establishing softening stress (σ)-crack opening displacement (w) relationship of concrete. In this paper, the bilinear expression for σ-w (see Figure 7) is chosen in the proposed numerical approach which is presented as follows:

According to Peterson [38], σ_s, w_s and w_0 can be determined as follows:

$$\sigma_s = f_t / 3 \tag{3}$$

$$w_s = 0.8G_F / f_t \tag{4}$$

$$w_0 = 3.6G_F / f_t \tag{5}$$

Where w_0 is the displacement of the terminal point of σ-w curve beyond which no stress can be transferred, i.e. the stress-free crack width, w_s and σ_s is the displacement and stress, respectively, corresponding to the break point in the bilinear σ-w relationship. These parameters and the σ-w relationship can be derived given the fracture energy G_F and the tensile strength f_t. Here, f_t is obtained from Equation (2) and G_F is from the formula recommended by CEB-FIP model code 2010.

Further, a crack propagation criterion based on nonlinear fracture mechanics is employed for predicting cracking propagation process in circular/elliptical concrete rings under restrained shrinkage. According to this criterion, when the SIF caused by deriving forces exceeds the one by cohesive forces, i.e. K_I^S-$K_I^\sigma \geq 0$, crack will propagate. It represents the competition between the crack driving forces which attempt to open the crack and the cohesive forces which attempt to close the crack [39]. This criterion has been successfully used to simulate the crack propagation in reinforced concrete [40], mode-I and mixed-mode fracture [41, 42] and multiple cohesive crack propagation [43] in concrete. In this study, SIFs caused by deriving forces, i.e. shrinkage effect, and cohesive force are denoted as K_I^S and K_I^σ, respectively. Moreover, in this study, the age-

dependent effective elastic modulus of concrete adopted in numerical analyses was taken as 60% of the value obtained from Equation (1) to account for creep effects. Similar measure in taking into account creep effect by reducing elastic modulus was also taken by [14, 30] when analyzing cracking in circular/elliptical concrete rings under restrained shrinkage. In numerical analysis, singular element was used to calculate SIF at the tip of crack. In order to eliminate the effect of friction between concrete and steel, the outer circumferential surface of the steel ring, which contacts the inner circumferential surface of the concrete ring, was coated with a release agent as suggested by ASTM C1581/C1581M-09a when preparing ring tests. Accordingly, in numerical analyses, contact element with zero friction between the contact pair was utilized to simulate this measure in conducting concrete ring tests.

In summary, the following steps were taken in analyzing crack initiation and propagation of a concrete ring subject to restrained shrinkage:

(1) Measure mechanical properties, including f_t and E, of concrete and free shrinkage through a series of concrete prisms with different A/V ratios at various ages. Convert the results of free shrinkage into a relationship between fictitious temperature drop and A/V ratio for a concrete element at various ages.
(2) Derive the fictitious temperature drop for a circular/elliptical ring specimen at various ages by linear interpolation from the relationship between fictitious temperature drop and A/V ratio obtained in step (1).
(3) Conduct an elastic analysis in a concrete ring by applying the corresponding fictitious temperature drop obtained in Step (2) on it, until the maximum circumferential tensile stress of concrete exceeds its tensile strength. Pre-set a 2

mm long fictitious crack on the location where the maximum circumferential tensile stress occurs in a circular/elliptical concrete ring.

(4) Apply cohesive stress on the fracture process zone (FPZ) according to the σ-w relationship. Calculate SIFs at crack tip caused by the cohesive force and shrinkage effect at various ages until K_I^S exceeds K_I^σ.

(5) Add an increment of crack length Δa=2 mm and repeat Step (4) and (5) until crack propagates throughout the section of the concrete ring wall.

4 Results and discussions

According to the numerical analysis results of Zhou et al. [30], the maximum circumferential tensile stress of concrete exceeds its tensile strength at the ages of 12 days for elliptical rings with R_1=150 mm and R_2=75 mm. In the case of circular rings with R_0=150 mm, the cracking age is 15 days. After crack initiation, a pre-crack is located on inner circumference of a circular ring, and the pre-crack is close to the vertices on the major axis of the inner circumference for an elliptical ring. There is cohesive stress acting on the pre-crack, which can be determined by the σ-w relationship specified in Figure 7. Figure 8 illustrates the pre-crack locations in circular and elliptical rings adopted in this study.

In order to elaborate crack propagation after initiation, Figures 9 and 10 present the evolution of SIF caused by shrinkage effect and cohesive stress in circular/elliptical concrete rings. For the circular ring with R_0=150 mm at the cracking age of 15 days, the SIFs at the tip of 2 mm pre-crack satisfy the criterion of K_I^S - K_I^σ=0, which suggests that the crack driving force caused by shrinkage effect can overcome the resistance caused by cohesive force. So the crack can propagate further under that condition.

While, $K_I^S - K_I^\sigma < 0$ (See Point A in Figure 9a) when the crack propagates to the length of 4 mm, it indicates that the resistance exceeds the crack driving force and the crack cannot propagate further. So in order that the crack is able to move forward, it is necessary to enhance the shrinkage effect of concrete, i.e. the crack driving energy. When concrete gets mature, i.e., from the 15th to the 16th day, the relationship between K_I^S and K_I^σ evolves to $K_I^S - K_I^\sigma > 0$ corresponding to a crack length of a=4 mm (See Point B in Figure 9b). Moreover, at the age of 16 days, K_I^S becomes always greater than K_I^σ and the difference between K_I^S and K_I^σ (i.e. $K_I^S - K_I^\sigma$) keeps increasing with the increase of crack length. This demonstrates that the crack driving force exceeds the resistance which is the cohesive stress tending to close the crack and the crack will propagate throughout the concrete ring wall at the 16th day. Comparing with the scenario of monotonic increasing of K_I^S with the increase of crack length, there are three distinguished stages in the evolution of K_I^σ, i.e., monotonically increasing before crack length reaches 14 mm (i.e. $a \leq 14$ mm), keeping plateaued when crack length is between 14 and 24 mm (i.e. a= 4~24 mm), and monotonically decreasing when crack length exceeds 24 mm (i.e. a>24 mm). The variation of K_I^σ can be explained by the shortening of FPZ when the crack tip is closed to the outer circumferential surface of a concrete ring.

For the elliptical ring with R_1=150 mm and R_2=75 mm, when crack initiates at the age of 12 days, $K_I^S - K_I^\sigma = 0$ corresponding to a crack length a=2 mm. It indicates that the crack can continue propagating under that condition. In numerical analysis, a new crack length in this case 4 mm is reached by giving a crack length increment Δa=2 mm to the original crack length 2 mm. However, when crack propagates to 4 mm long, it reaches a different scenario. In this case, SIF caused by cohesive force, i.e. K_I^σ, becomes greater than that caused by the driving force, i.e. K_I^S, which in fact is due to shrinkage effect. It

388 indicates that the crack cannot propagate further until the driving force can be enhanced
389 and SIF caused by driving force, i.e. K_I^{σ}, becomes greater than SIF caused by cohesive
390 force, i.e. K_I^{σ}. As concrete gets mature as drying continues, the accumulative shrinkage
391 effect keeps increasing. At the age of 13 days, K_I^{S} eventually becomes greater than K_I^{σ}
392 and the deviation between K_I^{S} and K_I^{σ} becomes greater than 0 thereafter. Therefore the
393 crack will keep propagating till throughout the concrete ring wall.

394 Besides, before crack starts unstable propagation, the maximum value of K_I^{S} - K_I^{σ}
395 occurs at the crack length of a=4 mm for a circular ring (See Point A in Figure 9a), and
396 a=8 mm for an elliptical ring (See Point A in Figure 10a). Within one day after crack
397 initiates, it can propagate throughout the concrete ring wall. At the corresponding points
398 B in Figures 9b and 10b, K_I^{S} becomes greater than K_I^{σ}. Therefore, it can be concluded
399 that the crack lengths at the onset of unstable propagation for circular and elliptical
400 rings are 4 and 8 mm, respectively. The difference in crack length at the onset of
401 unstable propagation in circular and elliptical concrete rings is due to the difference in
402 stress gradient across a concrete ring wall with circular and elliptical geometries.
403 Comparing with a circular ring geometry, the stress gradient in a concrete wall is more
404 significant for an elliptical ring geometry [30]. Meanwhile, the stable propagation
405 length gives a reference to determine an appropriate pre-crack length a_0 for numerical
406 analysis of concrete rings under restrained shrinkage. For example, in the case of a
407 circular ring, the stable propagation of concrete crack cannot be captured by numerical
408 analysis once a_0 exceeds 4 mm under current study condition.

409 In the standard restrained ring test methods recommended by AASHTO T334-08
410 and ASTM C1581/C1581M-09a, compressive strain developed in a steel ring caused
411 by shrinkage of mortar or concrete surrounding it is monitored by stain gauges attached
412 on the inner circumferential surface of the steel ring. As concrete is getting mature, it

413 shrinks but is restrained by the inner steel ring. Therefore, tensile stress develops in the
414 concrete ring and compression stress in steel ring. Cracking of the concrete ring is
415 indicated by a sudden drop in the steel ring strain. However, it should be noted that the
416 sudden drop of steel ring strain only represents the release of restraint effect in concrete
417 caused by the inner steel ring, rather than explicitly reflects the statue of crack, i.e.
418 initiation, stable propagation or unstable propagation, in concrete. According to the
419 numerical results conducted in this study, for the purpose of crack propagation, the
420 restraining effect should be strengthened after crack initiation until the driving force
421 caused by restraint shrinkage becomes greater than the resistance force so that crack
422 can continue growing till propagating throughout the concrete ring wall. Therefore, the
423 sudden drop of steel ring strain observed in the test recommended by ASTM
424 C1581/C1581M-09a illustrates the crack unstable propagation, which is regarded as a
425 structural response, rather than the crack initiation, which is regarded as a crack
426 resistance of concrete as a material property. Structural response of a concrete element
427 does depend on its thickness. In this case, the cracking age of a restrained concrete ring
428 depends on its ring wall thickness. However, it should be noted that the period from
429 crack initiation to unstable propagation is very short, which is within one day, in both
430 circular and elliptical rings subject to restrained shrinkage for the cases investigated in
431 this study. Moreover, although K_{I}^{S} is smaller than K_{I}^{σ} after crack initiation, the
432 difference between K_{I}^{S} and K_{I}^{σ} is very marginal with the maximum value of 0.08
433 MPa·mm$^{1/2}$ in a circular ring (See Point A in Figure 9a) and 0.38 MPa·mm$^{1/2}$ in an
434 elliptical ring (See Point A in Figure 10a). These differences can be ignored compared
435 with the SIFs caused by restrained shrinkage effect, which are about 6.5 MPa·mm$^{1/2}$ in
436 both geometries. Therefore, it is reasonable to accept that restrained shrinkage ring test
437 can approximately determine crack resistance of concrete and other cement-based

materials as per AASHTO T334-08 and ASTM C1581/C1581M-09a. According to numerical analysis results, the cracking ages for circular and elliptical rings are 16 and 13 days, respectively, which are the age at the onset of crack unstable propagation. The experimental results of cracking ages with respective to the circular and elliptical rings are about 15 and 10 days, which are determined by a sudden drop in the steel ring strain. The cracking ages predicted through the numerical model agreed reasonably well with experimental results indicating that the proposed numerical model is reliable.

Further, it is well known that crack initiation in concrete can be regarded as material behavior on cracking resistance, which is independent of specimen geometry and boundary condition. However, unstable concrete crack propagation in a restrained concrete ring represents structural response to external stimulation, i.e. it is structure behavior, which depends on specimen geometry and boundary condition. In restrained shrinkage ring test, concrete crack actually experiences the full spectrum of initiation, stable propagation and unstable propagation till propagating throughout the ring wall. The observed sudden strain drop of an inner steel ring reports that a crack propagates throughout a concrete ring wall, i.e. unstable propagation. Then, the results obtained in the ring test indicate structural behavior of a concrete ring subject to restrained shrinkage, rather than material behavior of concrete as per the suggestions of the AASHTO T334-08 and ASTM C1581/C1581M-09a. It is worthy pointing out here that, from the point of view of applying the ring test to assess cracking tendency of concrete as a material property of concrete, the difference in ages at crack initiation (representing material behavior) and unstable propagation (representing structural behavior) is very marginal although the mechanical mechanism is distinguished.

5 Conclusions

In this study, crack initiation and propagation in restrained concrete rings, both circular and elliptical, is analyzed. A fictitious temperature drop is applied on concrete to simulate the shrinkage effect of concrete due to drying. Combined with the fictitious crack model, a numerical mode is established for investigating crack initiation and propagation in circular/elliptical concrete rings under restrained shrinkage for the purpose of assessing cracking tendency of concrete and other cement-based materials as per AASHTO T334-08 and ASTM C1581/C1581M-09a. The evolution of SIF caused by restrained shrinkage and cohesive force for circular and elliptical rings is investigated with respect to concrete age. Based on the results presented in this paper, the following conclusions can be drawn.

(1) The initial cracking ages predicted through the numerical model agree reasonably well with experimental results indicating that the proposed numerical model is reliable. The fracture-based method developed in this study can be employed for simulating crack propagation process in circular/elliptical concrete rings under restrained shrinkage.

(2) There is a stable crack propagation process after crack initiation in restrained circular/elliptical concrete rings. The sudden strain drop measured from the internal surface of a restraining steel ring in a standard ring test indicates that a crack propagates throughout the concrete ring wall. For both circular and elliptical rings in the cases studied of this paper, the crack initiation and propagation throughout the concrete ring wall do not occur at the same time. Concrete cracks can propagate through a ring wall within one day after initiation. However, it should be noted here that the time, from crack initiation to propagation throughout a concrete ring wall,

depends on the type of concrete and the geometry of a ring specimen. In certain cases, this can be much longer than 1 day.

(3) The cracking age of concrete or other cement-based materials, which is characterized as a crack propagating throughout the concrete ring wall in a restrained ring test, depends on the degrees of restraint, resulted from the properties of steel and concrete (i.e. elastic modulus, Poisson's ratio etc.), and the geometry of the ring specimen (i.e. radius of steel ring, thickness of steel and concrete rings, etc.) [14]. So results given by the AASHTO/ASTM restrained ring test actually reflects the response of a concrete ring as a structure to external stimulation, in this case restrained concrete shrinkage. Thus the AASHTO/ASTM restrained ring test actually provides information about the structural behavior of a restrained concrete ring, rather than material behavior of concrete as per the suggestions of the AASHTO T334-08 and ASTM C1581/C1581M-09a.

Acknowledgements

The financial support from the National Natural Science Foundation of China under the grants of NSFC 51478083 & 51421064, Engineering and Physical Sciences Research Council under the grant of EP/I031952/1, and the National Basic Research Program of China (973 Program, Grant No. 2015CB057703) is gratefully acknowledged.

References

1. Carlson RW, Reading TJ (1988) Model study of shrinkage cracking in concrete building walls. ACI Struct J 85 (4):395-404.
2. Gilbert RI (1992) Shrinkage cracking in fully restrained concrete members. ACI Struct J 89 (2):141-149.

3. Almudaiheem JA, Hansen W (1987) Effect of specimen size and shape on drying shrinkage of concrete. ACI Mat J 84 (2):130-135.
4. Malhotra VM, Zoldners NG (1967) Comparison of ring-tensile strength of concrete with compressive flexural and splitting-tensile strengths. Journal of Materials 2 (1):160.
5. Swamy RN, Stavrides H (1979) Influence of fiber reinforcement on restrained shrinkage and cracking. ACI Journal Proceedings 76 (3):443-460.
6. Branch J, Rawling A, Hannant DJ, Mulheron M (2002) The effects of fibres on the plastic shrinkage cracking of high strength concrete. Mater Struct 35 (3):189-194.
7. See HT, Attiogbe EK, Miltenberger MA (2003) Shrinkage Cracking Characteristics of Concrete Using Ring Specimens. ACI Mater J 100 (3):239-245.
8. Mokarem DW, Weyers RE, Lane DS (2005) Development of a shrinkage performance specifications and prediction model analysis for supplemental cementitious material concrete mixtures. Cem Concr Res 35 (5):918-925.
9. Passuello A, Moriconi G, Shah SP (2009) Cracking behavior of concrete with shrinkage reducing admixtures and PVA fibers. Cem Concr Comp 31 (10):699-704.
10. Tongaroonsri S, Tangtermsirikul S (2009) Effect of mineral admixtures and curing periods on shrinkage and cracking age under restrained condition. Constr Build Mater 23 (2):1050-1056.
11. Weiss WJ, Yang W, Shah SP (2000) Influence of Specimen Size/Geometry on Shrinkage Cracking of Rings. J Eng Mech 126 (1):93-101.
12. Moon JH, Weiss J (2006) Estimating residual stress in the restrained ring test under circumferential drying. Cem Concr Comp 28 (5):486-496.
13. Hossain AB, Weiss J (2006) The role of specimen geometry and boundary conditions on stress development and cracking in the restrained ring test. Cem Concr Res 36 (1):189-199.
14. Moon JH, Rajabipour F, Pease B, Weiss J (2006) Quantifying the influence of specimen geometry on the results of the restrained ring test. J ASTM Int 3 (8):1-14.
15. He Z, Zhou X, Li Z (2004) New Experimental Method for Studying Early-Age Cracking of Cement-Based Materials. ACI Mater J 101 (1):1-7.
16. He Z, Li Z (2005) Influence of alkali on restrained shrinkage behavior of cement-based materials. Cem Concr Res 35 (3):457-463.

542 17. He Z, Li ZJ, Chen MZ, Liang WQ (2006) Properties of shrinkage-reducing admixture-
543 modified pastes and mortar. Mater Struct 39 (4):445-453.
544 18. Ma BG, Wang XG, Liang WQ, Li XG, He Z (2007) Study on early-age cracking of cement-
545 based materials with superplasticizers. Constr Build Mater 21 (11):2017-2022.
546 19. Gao Y, Tang S, Zhang H, Liu H (2013) Study on early autogenous shrinkage and crack
547 resistance of fly ash high-strength lightweight aggregate concrete. Mag Concr Res 65
548 (15):906-913.
549 20. Pour-Ghaz M, Poursaee A, Spragg R, Weiss J (2011) Experimental Methods to Detect and
550 Quantify Damage in Restrained Concrete Ring Specimens. J Adv Concr Technol 9 (3):251-
551 260.
552 21. Yoo DY, Park JJ, Kim SW, Yoon YS (2014) Influence of ring size on the restrained
553 shrinkage behavior of ultra high performance fiber reinforced concrete. Mater Struct 47
554 (7):1161-1174.
555 22. Zou D, Weiss J (2014) Early age cracking behavior of internally cured mortar restrained by
556 dual rings with different thickness. Constr Build Mater 66 (9):146-153.
557 23. Shah SP, Sheng. OC, Marikunte S, Yang W, Emilie. B-G (1998) A Method to Predict
558 Shrinkage Cracking of Concrete. ACI Mater J 95 (4):339-346.
559 24. Turcry P, Loukili A, Haidar K, Pijaudier-Cabot G, Belarbi A (2006) Cracking Tendency of
560 Self-Compacting Concrete Subjected to Restrained Shrinkage: Experimental Study and
561 Modeling. J Mater Civil Eng 18 (1):46-54.
562 25. Ouyang C, Mobasher B, Shah SP (1990) An R-curve approach for fracture of quasi-brittle
563 materials. Eng Fract Mech 37 (4):901-913.
564 26. Ouyang C, Shah SP (1991) Geometry-dependent R-curve for quasi-brittle materials J Am
565 Ceram Soc 74 (11):2831-2836.
566 27. Weiss WJ, Yang W, Shah SP (1998) Shrinkage cracking of restrained concrete slabs. J Eng
567 Mech ASCE 124 (7):765-774.
568 28. Weiss J (1999) Prediction of early-age shrinkage cracking in concrete. Northwestern
569 University
570 29. Dong W, Zhou X, Wu Z (2014) A fracture mechanics-based method for prediction of
571 cracking of circular and elliptical concrete rings under restrained shrinkage. Eng Fract

572 Mech 131 (12):687-701.
573 30. Zhou X, Dong W, Oladiran O (2014) Assessment of Restrained Shrinkage Cracking of
574 Concrete Using Elliptical Ring Specimens: Experimental and Numerical. J Mater Civil Eng
575 26 (12):871-878.
576 31. Hossain AB, Weiss J (2004) Assessing residual stress development and stress relaxation in
577 restrained concrete ring specimens. Cem Concr Comp 26 (5):531-540.
578 32. Shah HR, Weiss J (2006) Quantifying shrinkage cracking in fiber reinforced concrete using
579 the ring test. Mater Struct 39 (9):887-899.
580 33. Hillerborg A, Modéer M, Petersson PE (1976) Analysis of crack formation and crack
581 growth in concrete by means of fracture mechanics and finite elements. Cem Concr Res 6
582 (6):773-781.
583 34. Radlinska A, Bucher B, Weiss J (2008) Comments on the interpretation of results from the
584 restrained ring test. J ASTM Int 5 (10):1-12.
585 35. Schlitter JL, Senter AH, Bentz DP, Nantung T, Weiss WJ (2010) A Dual Concentric Ring
586 Test for Evaluating Residual Stress Development due to Restrained Volume Change. J
587 ASTM Int 7 (9):1-13.
588 36. Schlitter JL, Barrett T, Weiss J Restrained shrinkage behavior due to combined autogenous
589 and thermal effects in mortars containing super absorbent polymer (SAP). In: Jensen OM,
590 Hasholt OM, Laustsen S (eds) International RILEM Conference on Use of Superabsorbent
591 Polymers and Other New Additives in Concrete 2010. RILEM Publications SARL, pp 233-
592 242
593 37. Schlitter JL, Bentz DP, Weiss WJ (2013) Quantifying Stress Development and Remaining
594 Stress Capacity in Restrained, Internally Cured Mortars. ACI Mater J 110 (1):3-11.
595 38. Petersson PE (1981) Crack growth and development of fracture zones in plain concrete and
596 similar materials. Division of Building Materials, Lund Institute of Technology, Report
597 TVBM-1006, Sweden, 1981.
598 39. Moës N, Belytschko T (2002) Extended finite element method for cohesive crack growth.
599 Eng Fract Mech 69 (7):813-833.
600 40. Ooi ET, Yang ZJ (2011) Modelling crack propagation in reinforced concrete using a hybrid
601 finite element–scaled boundary finite element method. Eng Fract Mech 78 (2):252-273.

41. Yang ZJ, Deeks AJ (2007) Fully-automatic modelling of cohesive crack growth using a finite element–scaled boundary finite element coupled method. Eng Fract Mech 74 (16):2547-2573.
42. Ooi ET, Yang ZJ (2010) A hybrid finite element-scaled boundary finite element method for crack propagation modelling. Comput Method Appl M 199 (17-20):1178-1192.
43. Ooi ET, Yang ZJ (2009) Modelling multiple cohesive crack propagation using a finite element–scaled boundary finite element coupled method. Eng Anal Bound Elem 33 (7):915-929.

Figure captions.

Figure 1. Free shrinkage test setup

Figure 2. Shrinkage strain of concrete obtained from free shrinkage test

Figure 3. Notation of geometrical parameters; **a** circular ring, **b** elliptical ring

Figure 4. Restrained shrinkage ring test; **a** test setup for an elliptical ring, **b** sealed specimens

Figure 5. Derived fictitious temperature drop with respect to A/V ratio for a concrete element

Figure 6. Crack position in an elliptical ring specimen

Figure 7. Bilinear σ-w softening curve for concrete

Figure 8. Pre-crack in concrete rings; **a** circular, **b** elliptical

628 Figure 9. Evolution of SIFs in a circular ring at the ages of crack initiation and unstable
629 propagation; **a** 15 days, **b** 16 days
630 Figure 10. Evolution of SIFs in an elliptical ring at the ages of crack initiation and
631 unstable propagation; **a** 12 days, **b** 13 days

632

633

634 **Fig. 1.** Free shrinkage test setup

635

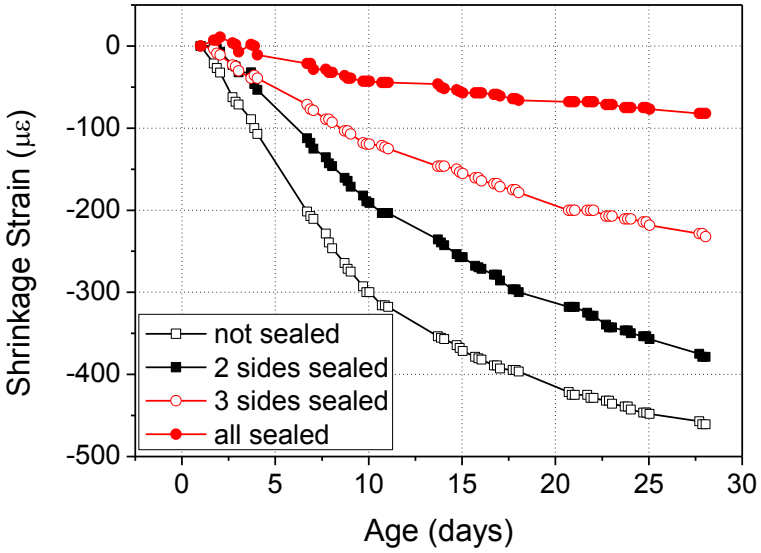

636

637 **Fig. 2.** Shrinkage strain of concrete obtained from free shrinkage test

638

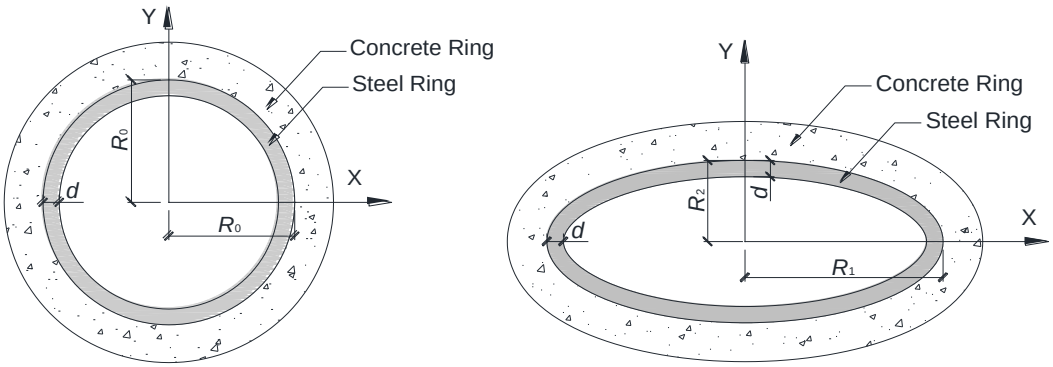

(a) (b)

Fig. 3. Notation of geometrical parameters; **a** circular ring, **b** elliptical ring

643 

644 (a) (b)

645 **Fig. 4.** Restrained shrinkage ring test; **a** test setup for an elliptical ring, **b** sealed specimens

646

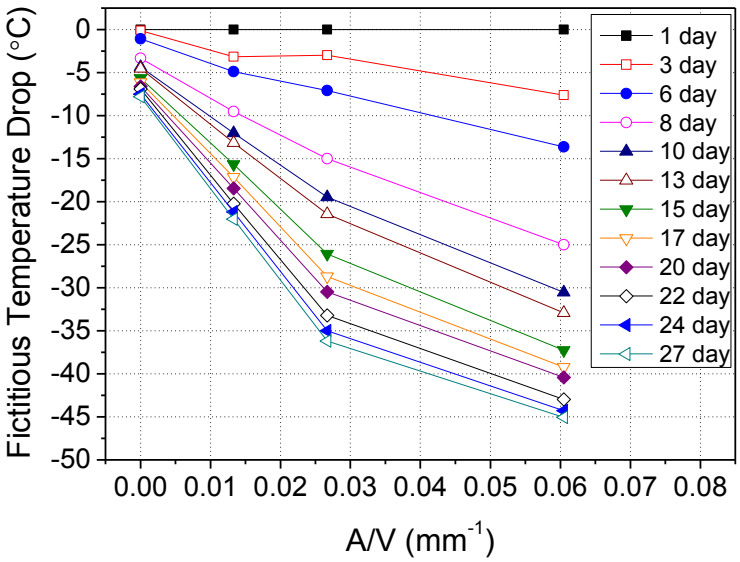

647

648 **Fig. 5.** Derived fictitious temperature drop with respect to A/V ratio for a concrete element

649

650

651 **Fig. 6.** Crack position in an elliptical ring specimen

652

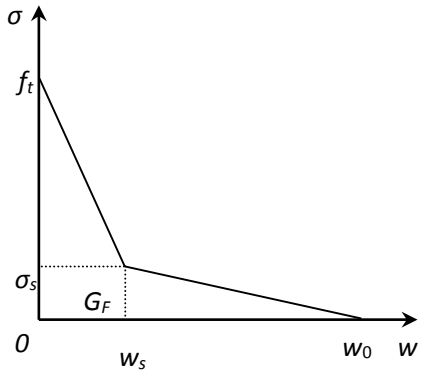

Fig. 7. Bilinear σ-w softening curve for concrete

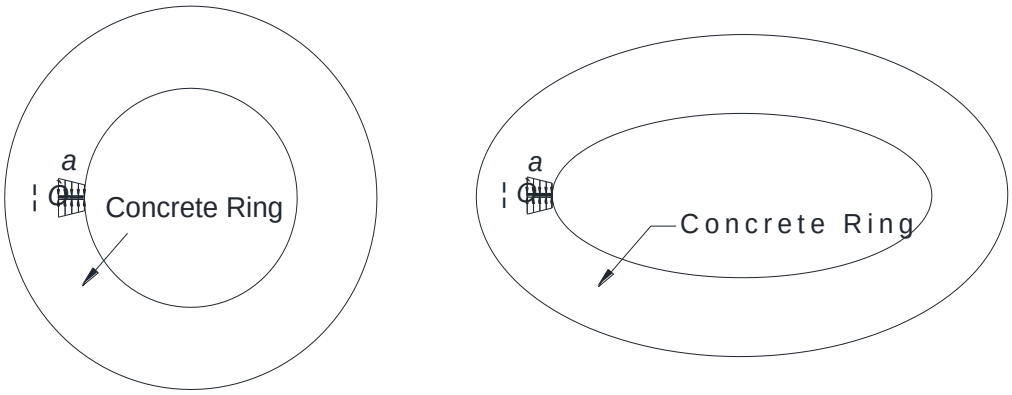

(a) (b)

Fig. 8. Pre-crack in concrete rings; **a** circular, **b** elliptical

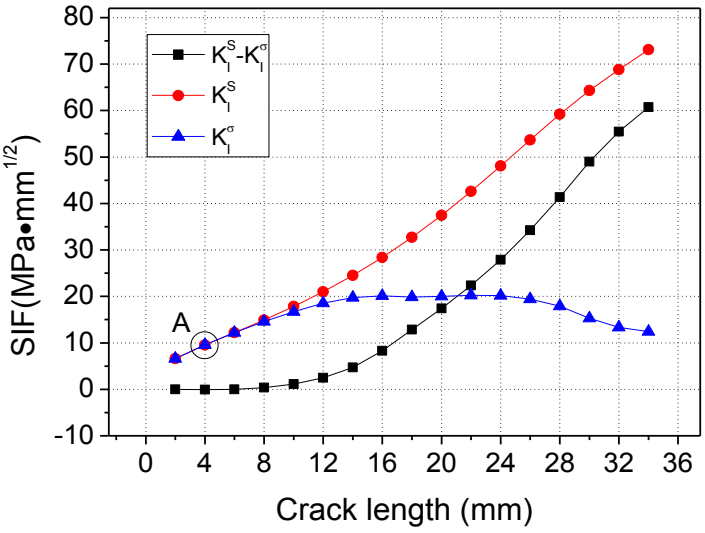

(a)

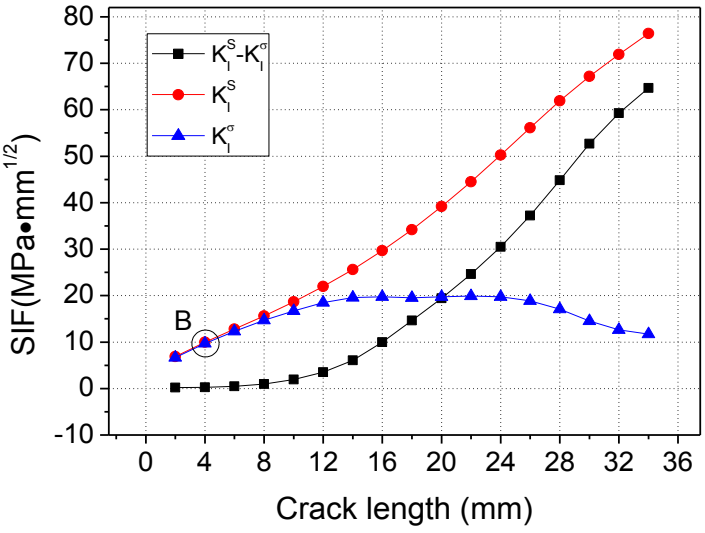

(b)

Fig. 9. Evolution of SIFs in circular ring at the ages of crack initiation and unstable propagation; **a** 15 days, **b** 16 days

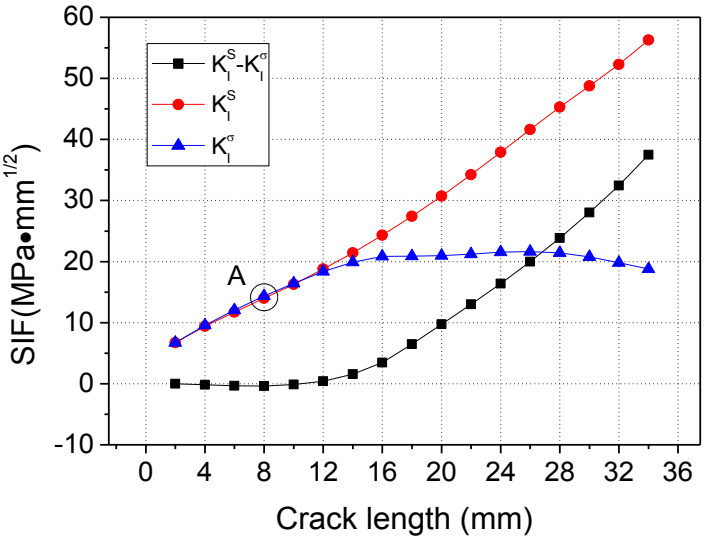

667

668 (a)

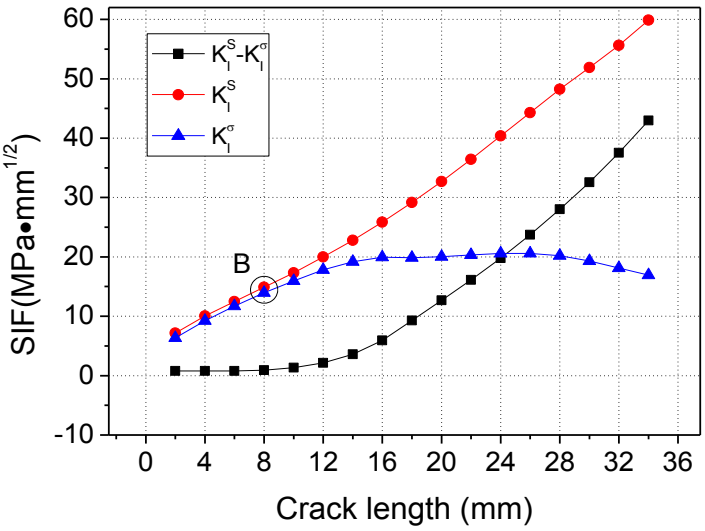

669

670 (b)

671 **Fig. 10.** Evolution of SIFs in elliptical ring at the ages of crack initiation and unstable propagation; **a**

672 12 days, **b** 13 days